

Quantum dot spectroscopy of proximity-induced superconductivity in a two-dimensional electron gas

F. Deon,^{1,*} V. Pellegrini,¹ F. Giazotto,¹ G. Biasiol,² L. Sorba,¹ and F. Beltram¹

¹*NEST, Istituto Nanoscienze-CNR and Scuola Normale Superiore, I-56127 Pisa, Italy*

²*CNR-IOM, Laboratorio TASC, Area Science Park, I-34149 Trieste, Italy*

(Dated: July 31, 2021)

We report the realization of a hybrid superconductor-quantum dot device by means of top-down nanofabrication starting from a two dimensional electron gas in a InGaAs/InAlAs semiconductor heterostructure. The quantum dot is defined by electrostatic gates placed within the normal region of a planar Nb-InGaAs quantum well-Nb junction. Measurements in the regime of strong Coulomb blockade as well as cotunneling spectroscopy allow to directly probe the proximity-induced energy gap in a ballistic two-dimensional electron gas coupled to superconductors.

Hybrid devices in which a quantum dot (QD) is connected to superconducting (S) electrodes display a rich physical behavior, which stems from the coexistence of competing phenomena such as proximity superconductivity, Coulomb blockade and the Kondo effect¹. Several examples of hybrid QD devices have been demonstrated so far, all of which rely on nanostructures defined by bottom-up approaches such as carbon nanotubes², semiconductor nanowires³ and self-assembled QDs^{4,5}. Transport studies in these nanosystems have demonstrated Josephson currents in S-QD-S devices and tuning of the critical current by changing the QD charge state^{6,7}. Other authors have focused on quasiparticle transport, in particular on the interplay of Coulomb blockade, superconducting order in the leads and Kondo effect^{8,9}.

In the perspective of practical implementations, large-scale integrability is a key requirement, and a top-down nanofabrication approach based on two dimensional electron gases (2DEGs) confined in semiconductor heterostructures would be preferable. Finally, QDs embedded into 2DEG-based hybrid structures can be used as a spectroscopic tool of proximity-induced superconductivity in ballistic electronic systems. While the local density of states (DOS) in proximized normal metal films has been probed using weakly-coupled tunnel contacts^{10,11}, a similar measurement in the case of the 2DEG hosted in a ballistic semiconductor heterostructure has not been performed to date.

In this letter we report the realization of a hybrid S-QD-S device by means of top-down nanofabrication, starting from a 2DEG confined in a In_{0.80}Ga_{0.20}As/In_{0.75}Al_{0.25}As heterostructure. Following previous work¹²⁻¹⁴, the QD is formed by applying negative voltages to surface electrostatic gates placed on top of a narrow mesa strip etched in the heterostructure, and laterally contacted by superconducting niobium electrodes. We discuss the impact of the proximity-induced superconductivity on the transport properties in different regimes of coupling to the leads, and measure the proximity-induced energy gaps in the two-dimensional electron gas.

A scanning electron micrograph and the main nanofabrication steps are shown in Fig. 1(a,b). The active

region of the heterostructure contains a 15 nm-thick δ -doped In_{0.80}Ga_{0.20}As quantum well^{15,16}, sandwiched between In_{0.75}Al_{0.25}As barriers. The sheet electron density, measured from the period of Shubnikov - de Haas oscillations, is $n_S \simeq 5.9 \times 10^{11} \text{ cm}^{-2}$. The mobility $\mu \simeq 1.8 \times 10^5 \text{ cm}^2 \text{ V}^{-1} \text{ s}^{-1}$ is equivalent to an electron mean free path $l_p \simeq 2.3 \mu\text{m}$. InAs and In_xGa_{1-x}As alloys with high molar fraction $x \geq 0.75$ have often been used in association with Nb for the realization of hybrid ballistic devices, thanks to their property of forming Schottky barrier-free junctions. For the same reason a suitable dielectric is required for the electrical insulation of the electrostatic gates.

The nanofabrication of the hybrid device requires several mutually-aligned steps of electron beam lithography (EBL). First [Fig. 1(a1)] we pattern a dielectric strip on the heterostructure surface, by means of EBL, using hydrogen silsesquioxane (HSQ) as a negative tone e-beam resist¹⁷. Thickness and width of the strip are 60 nm and 600 nm, respectively. The mesa strip is defined by wet etching in a H₃PO₄-H₂O₂ solution through an EBL-patterned poly(methyl methacrylate) mask (a2). Electrostatic gates are then added by thermal evaporation and liftoff (a3), followed by sputtering and liftoff of the Nb side contacts (a4). The junction has a width $W = 3.0 \mu\text{m}$, while the inter-electrode distance, equal to the width of the etched mesa strip, is $L = 650 \text{ nm}$. In order to maximize interface transmissivity, the native oxide and possible contaminants must be removed from the mesa sidewalls before the deposition of the contacts. To this end we perform low-energy Ar⁺ sputter-cleaning in high vacuum, immediately before the deposition of Nb^{18,19}.

Low temperature measurements are performed down to 150 mK. Below the critical temperature $T_c \approx 9 \text{ K}$ of the Nb films, proximity-induced superconductivity²⁰ in the semiconductor modifies the DOS at energies $|\epsilon| \lesssim \Delta$ (where $\Delta = 1.764 k_B T_c \simeq 1.35 \text{ meV}$ is the superconducting gap of the Nb films and k_B the Boltzmann constant). The normal-state resistance of the junction is $R_N = 150 \Omega$, roughly two times larger than the lower bound set by the Sharvin resistance $R_{Sh} = (\pi h)/(2e^2 W \sqrt{2\pi n_S}) = 70 \Omega$, where h is Planck's con-

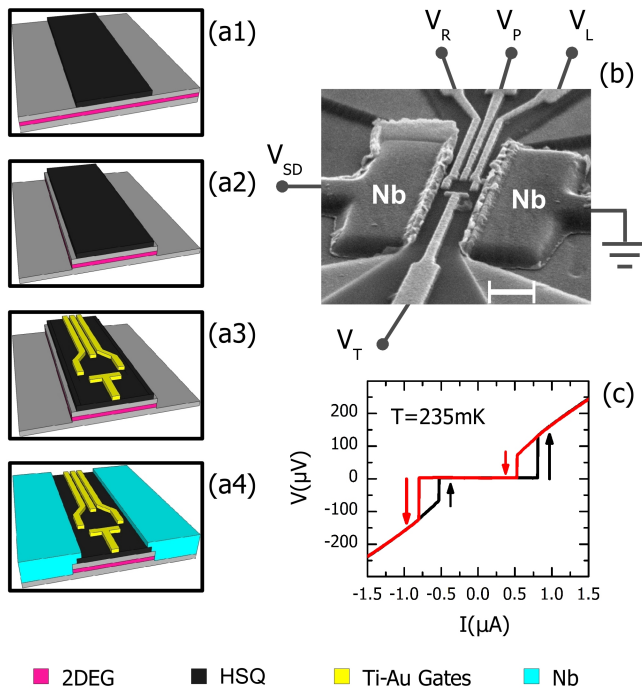


FIG. 1: **Device layout.** (a1-4) Summary of the main nanofabrication steps and cross-sectional schematics of the hybrid superconductor-quantum dot device. (b) Scanning electron micrograph of the sample (scale bar is 500 nm). (c) Voltage-current characteristic at $T = 235 \text{ mK}$ of the open Nb-InGaAs-Nb junction (all gates set to ground).

stant. The voltage-current characteristic²¹ of the open junction (all gates set to ground), measured at 235 mK, is plotted in Fig. 1(c) and shows a switching current $I_c \simeq 800 \text{ nA}$. We note that in this configuration the junction length L is smaller than the electron scattering length l_p and larger than the induced coherence length $\xi_N = (\hbar^2 \sqrt{2\pi n_S}) / (\Delta m^*) = 360 \text{ nm}$ (where $m^* = 0.03 m_e$ is the electron effective mass in $\text{In}_{0.80}\text{Ga}_{0.20}\text{As}$), so that the normal region is ballistic and the junction falls in the intermediate length regime.

When negative voltages V_L , V_R and V_T are applied to the electrostatic gates [see Fig. 1(b)], the underlying 2DEG regions are depleted, forming a QD. The voltage V_P applied to the fourth gate allows to tune the charge state of the QD. Two point-contacts with tunable transparency couple the QD island to the nearby Nb-InGaAs (S-2DEG) junctions. The distance between the Nb-InGaAs interfaces and the electrostatic gates that define the QD is of the order of 100 nm, below the induced coherence length ξ_N . For superconductor-normal metal (SN) junctions with a normal region length approaching or smaller than ξ_N the proximity-induced energy gap Δ^* is expected to increase, reaching Δ in the case of ideal NS interfaces in the short junction limit; a suppression of Δ^* should occur for contacts with finite interface transparency²³. It is known that the stability diagram of

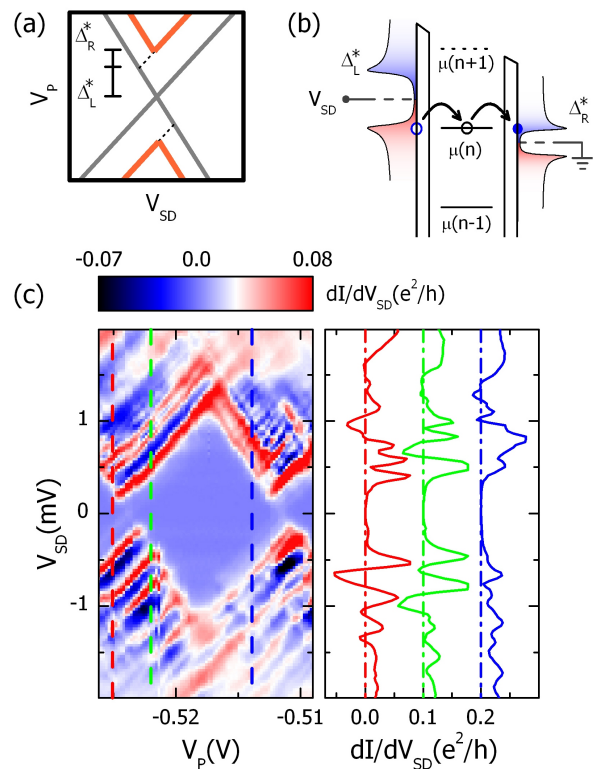


FIG. 2: **Stability diagram for the closed QD.** (a) Sketch of the Coulomb diamond edges in the case of normal leads (gray lines) and in the presence of proximity-induced gaps Δ_L^* and Δ_R^* . (b) energy diagram for single electron tunneling in the hybrid QD. (c) Left panel: color plot of the differential conductance versus V_{SD} and V_P (stability diagram) in the case of weak coupling to the leads at $T = 235 \text{ mK}$. Right panel: dI/dV_{SD} traces for three values of plunger gate voltage V_P (indicated by dashed lines in the stability plot). The curves are horizontally shifted for clarity: dot-dashed lines indicate $dI/dV_{SD} = 0$.

a QD directly connected to superconductors reveals the presence of a gap in the DOS, both for weak and strong tunnel coupling to the leads^{4,9,24}. We will show in the following that our device can be easily tuned between the two regimes, and report our measurement of Δ^* in the 2DEG.

Figure 2(a) shows measurements ($T = 235 \text{ mK}$) in a regime of weak QD-lead coupling: the QD differential conductance dI/dV_{SD} is plotted in color scale as a function of the source-drain bias V_{SD} and V_P (stability plot). In the diamond-shaped regions of low conductance electron tunneling through the QD is forbidden by Coulomb repulsion, and the QD occupation number n is constant. Diamond edges with positive (negative) slope correspond to the onset of single electron tunneling from the left (right) lead. A sketch of the stability plot is given in Fig. 2(b): in the case of normal contacts (gray lines) the diamond edges cross at $V_{SD} = 0$, forming zero bias Coulomb blockade peaks at the charge-degeneracy points. The presence of gaps Δ_L^* and Δ_R^* in the DOS

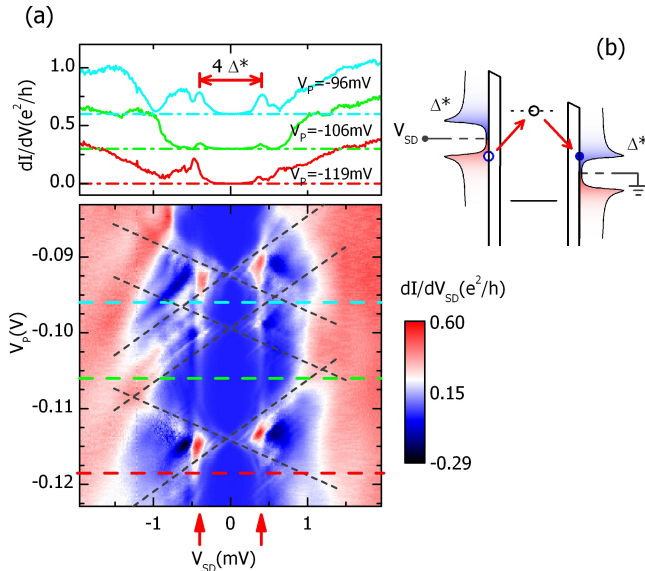


FIG. 3: **Cotunneling spectroscopy.** (a) Stability diagram in the regime of stronger QD-lead coupling at $T = 150$ mK: symmetric peaks (indicated by the red arrows) appear inside the diamonds at constant voltages $V_{SD} = \pm 2\Delta^*/e$ (independent of V_P), where the electron- and hole-like DOS peaks enhance the onset of elastic processes. One of such cotunneling processes is sketched in panel (b). Differential conductance profiles for three values of V_P (indicated by dashed lines in the stability plot) are displayed in the upper panel. The curves are vertically shifted for clarity: dot-dashed lines in the upper panel indicate $dI/dV_{SD} = 0$.

of the left and right lead, respectively, shifts the onset of the corresponding diamond edges [orange lines in Fig. 2(b)] to higher values of $|V_{SD}|$ [see Fig. 2(c)]. The measured values of Δ_L^* and Δ_R^* are $\Delta_L^* = (180 \pm 10)\mu\text{eV}$ and $\Delta_R^* = (15 \pm 10)\mu\text{eV}$. Such a large asymmetry could be linked to asymmetric tunnel coupling of the QD to the leads and to the consequent asymmetric depletion and weakening of the proximity effect in the adjacent 2DEG regions. Our finding that $\Delta_L^* \gg \Delta_R^*$ is also consistent with the fact that excited-state lines pertaining to the

left lead are more intense and followed by regions of large negative dI/dV_{SD} ⁹.

Our device architecture allows to easily tune the QD to a regime of stronger coupling to the leads by increasing the voltages V_L , V_R , V_T of a few mV. In this regime cotunneling processes lead to the appearance of finite conductance inside the Coulomb diamonds [see Fig. 3(a)]. Symmetric peaks in dI/dV_{SD} located at a constant voltage $V_{SD} = 330 \mu\text{V}$, independent of the charge state of the QD, are due to elastic cotunneling processes, such as the one sketched Fig. 3(b). In the upper panel of Fig. 3(a) the differential conductance is plotted versus V_{SD} for constant values of V_P indicated by the dashed lines of corresponding color in the lower panel. In this case our data indicate that $\Delta_L^* = \Delta_R^* \equiv \Delta^*$: the onset of elastic cotunneling takes place at $|eV_{SD}| = 2\Delta^*$, where the particle- and hole-like DOS peaks in the two leads are aligned. We thus find $\Delta^* = 165 \mu\text{eV}$. This value is slightly smaller than the value of Δ_L^* found in the weak coupling regime (the difference being comparable with the uncertainty on Δ_L^*). We note that the data shown in Fig. 2 and Fig. 3 were taken in different cooldowns of the device, and a fluctuation in n_S could explain a variation in the strength of the proximity effect.

In conclusion, we demonstrated a hybrid QD device obtained by means of standard top-down nanofabrication, which combines a Nb-In_{0.8}Ga_{0.2}As-Nb planar junction with a lateral QD confined by electrostatic gates. Transport measurements allow to directly measure a proximity-induced gap in the 2DEG which results of the order of $200 \mu\text{eV}$. As these results are relevant to the development of non-dissipative single electron transistors, further work will be devoted to the study of Josephson coupling through our device.

The authors would like to thank P. Spathis for fruitful discussions and for help with the cryogenic setup. We acknowledge partial financial support from the E.U. Project HYSWITCH (grant No. FP6-517567), the MIUR-FIRB No. RBIN06JB4C, the INFN-CNR Seed project ‘Quantum dot refrigeration: accessing the μK regime in solid-state nanosystems’, and the NanoSciERA project ‘NanoFridge’.

* Electronic address: f.deon@sns.it

¹ S. De Franceschi, L. Kouwenhoven, C. Schönberger, and W. Wernsdorfer, *Nat. Nano.* **5**, 703 (2010).

² M. R. Buitelaar, T. Nussbaumer, and C. Schönberger, *Phys. Rev. Lett.* **89**, 256801 (2002).

³ T. Sand-Jespersen, J. Paaske, B. M. Andersen, K. Grove-Rasmussen, H. I. Jørgensen, M. Aagesen, C. B. Sørensen, P. E. Lindelof, K. Flensberg, J. Nygård, *Phys. Rev. Lett.* **99**, 126603 (2007).

⁴ K. Shibata, C. Buizert, A. Oiwa, K. Hirakawa, and S. Tarucha, *Appl. Phys. Lett.* **91**, 112102 (2007).

⁵ G. Katsaros, P. Spathis, M. Stoffel, F. Fournel, M. Mongillo, V. Bouchiat, F. Lefloch, A. Rastelli, O. G.

Schmidt, S. De Franceschi, *Nat. Nano.* **5**, 458 (2010).

⁶ J. A. van Dam, Y. V. Nazarov, E. P. Bakkers, S. De Franceschi, and L. P. Kouwenhoven, *Nature* **442**, 667 (2006).

⁷ H. Ingerslev Jørgensen, T. Novotny, K. Grove-Rasmussen, K. Flensberg, and P. Lindelof, *Nano Lett.* **7**, 2441 (2007).

⁸ A. Eichler, M. Weiss, S. Oberholzer, C. Schönberger, A. Levy-Yeyati, J. C. Cuevas, A. Martín-Rodero, *Phys. Rev. Lett.* **99**, 126602 (2007).

⁹ Y.J. Doh, S. De Franceschi, E. Bakkers, and L. P. Kouwenhoven, *Nano Lett.* **8**, 4098 (2008).

¹⁰ S. Gueron, H. Pothier, N.O. Birge, D. Esteve and M.H. Devoret, *Phys. Rev. Lett.* **77**, 3025 (1996).

- ¹¹ H. le Sueur, P. Joyez, H. Pothier, C. Urbina, and D. Esteve, *Phys. Rev. Lett.* **100**, 197002 (2008).
- ¹² H. Takayanagi, T. Akazaki, J. Nitta, *Phys. Rev. Lett.* **75**, 3533 (1995).
- ¹³ T. Bauch, E. Hürfeld, V. M. Krasnov, P. Delsing, H. Takayanagi, T. Akazaki, *Phys. Rev. B* **71**, 174502 (2005).
- ¹⁴ F. Deon, V. Pellegrini, F. Carillo, F. Giazotto, G. Biasiol, L. Sorba, F. Beltram, *Appl. Phys. Lett.* **96**, 142107 (2010).
- ¹⁵ F. Capotondi, G. Biasiol, D. Ercolani, V. Grillo, E. Carlino, F. Romanato, and L. Sorba, *Thin Solid Films* **448**, 400 (2005).
- ¹⁶ W. Desrat, F. Giazotto, V. Pellegrini, F. Beltram, F. Capotondi, G. Biasiol, and L. Sorba, *Phys. Rev. B* **69**, 245324 (2004).
- ¹⁷ D. Lauvernier, J. P. Vilcot, M. François, and D. Decoster, *Microelectr. Eng.* **75**, 177 (2004).
- ¹⁸ F. Giazotto, K. Grove-Rasmussen, R. Fazio, F. Beltram, E. H. Linfield, and D. A. Ritchie, *J. of Supercond.* **17**, 317 (2004).
- ¹⁹ The Fermi wavevector mismatch between Nb and the 2DEG also negatively affects interface transparency..
- ²⁰ B. Pannetier and H. Courtois, *J. of Low Temp. Phys.* **118**, 599 (2000).
- ²¹ The observed hysteresis is typical of S-N-S proximity junctions with high critical current density²².
- ²² H. Courtois, M. Meschke, J. Peltonen, and J. Pekola, *Phys. Rev. Lett.* **101**, 057005 (2008).
- ²³ J.C. Hammer, J.C. Cuevas, F.S. Bergeret, and W. Belzig, *Phys. Rev. B* **76**, 064514 (2007).
- ²⁴ A.L. Yeyati, J.C. Cuevas, A. Lopez-Davalos, A. Martín-Rodero, *Phys. Rev. B* **55**, R6137 (1997).